Regular Article

INORGANIC CHEMISTRY RESEARCH
Published by the
Iranian Chemical Society
www.inorgchemres.org
info@inorgchemres.org

Inorg. Chem. Res., Vol. 2, No. 1, 40-49, June 2019
DOI: 10.22036/icr.2019.194182.1052

Surface-grafted Europium and Erbium Complexes of the 12-Tungstosilicate Heteropolyoxometalate: A Synthetic and Structural Investigations

S. Derakhshanrad[a], M. Mirzaei[a,*] and J.T. Mague[b]

[a]*Department of Chemistry, Faculty of Science, Ferdowsi University of Mashhad, Mashhad, Iran*

[b]*Department of Chemistry, Tulane University, New Orleans, LA 70118, USA*

(Received 14 July 2019, Accepted 15 July 2019)

The hydrothermal synthesis of two new inorganic-organic hybrid materials in which PDA (PDA = 1,10-phenanthroline-2,9-dicarboxylate) is connected to a well-defined Keggin-type polyoxometalate anion (POM) and a Ln(III) cation (POM = $[SiW_{12}O_{40}]^{4-}$; Ln = Eu^{3+} (1), Er^{3+} (2)), are reported. These hybrids are characterized by elemental analyses, IR spectra and single-crystal X-ray diffraction. Single-crystal X-ray analysis reveals that both compounds have been assembled by hydrogen bonding and anion-π interactions among POM, PDA and lattice water units into a three-dimensional (3D) supramolecular structure. Compound 1 is composed of two different cationic layers of Eu(III) clusters with the POMs located in cavities that are created by the Eu-PDA groups. Compound 2 consists of $[SiW_{12}O_{40}]^{4-}$ Keggin-type POMs, where a single $\{W_3O_{13}\}$ triad is decorated by a trinuclear Er(III)-complex.

Keywords: Polyoxometalate, Phenanthroline, Lanthanoid, Inorganic-organic hybrid, X-ray

INTRODUCTION

In recent years, the design and synthesis of inorganic-organic hybrid materials based on polyoxometalates (POMs) have aroused considerable attention in the field of material science due to their potential applications and excellent properties in catalysis, magnetism, electrochemistry, biochemistry, photochemistry and material science [1-15]. Especially, with the advent of modern high-resolution and sophisticated instrumentation, the number of POM-based functional solid materials has been expanding at an explosive rate [16-19]. As a class of valuable inorganic building blocks, POMs not only have structural diversity and rich coordination modes but also can bring special properties to the hybrid materials [20,21]. Therefore, combining POMs with organic-metal coordination complexes can be a rational approach for preparing POM-based inorganic-organic hybrid materials which may incorporate the merits of both components. In order to construct this kind of hybrid material, the rational design and selection of a suitable ligand to tie the metal complex to the POM is a crucial factor [22,23]. To date, the bridging ligands employed contained N, O or halogen atoms as the potential coordination sites [24-27]. The design and synthesis of such novel solid materials remain an attractive challenge because it is still difficult to determine the appropriate synthetic conditions, such as pH, ratio of reactants, reaction time and temperature, and so on among others [28].

From the outset, two of classifications have been proposed for these hybrids based on the interactions between organic and inorganic compounds. In the first class, electrostatic interactions, hydrogen bonds, and van der Waals interactions play an essential role and there is no covalent bond between the organic and inorganic components. In the other class, the organic and inorganic components are covalently bonded [6,9]. Typically, ligands containing N and O donor groups are used to synthesize organic-inorganic hybrid compounds. These groups can be protonated in acidic media and

*Corresponding author. E-mail: mirzaeesh@um.ac.ir

converted to cationic forms which provides a very favorable condition for electrostatic or covalent bonding with POMs. For this reason, phenanthroline ligands and their derivatives with donor groups at the 2 and 9 positions, *i.e.* alcohols, amides, carboxylates, and oximes are considered in the preparation of inorganic-organic hybrids [29].

1,10-Phenanthroline-2,9-dicarbaldehyde dioxime (H_2phendox or PDOX) ligands also play significant roles in the construction of inorganic-organic hybrids with novel structures and properties. Many metal-organic frameworks (MOFs) based on PDOX ligands exhibit intriguing topologies and interesting magnetic, absorptive and photophysical properties. For these reasons we chose the simple and rigid PDOX ligand as a multifunctional group to build POM-based inorganic-organic hybrids because it exhibits diverse coordination/bridging modes as reported recently for MOF derivatives. The PDOX ligand can provide four and two sequential electron-donating N and O-donors, respectively, to coordinate with metal atoms and it also possesses a small steric hindrance showing the superiority in the construction of multinuclear clusters and high dimensional structures [28-31].

POMs, as a vast class of discrete anionic metal oxides, are usually generated via the condensation of metal oxide polyhedral (MO_x, M = W^{VI}, Mo^{VI}, V^{V}, Nb^{V}, Ta^{V}, *etc.*, x = 4-7) in corner-, edge-, or face-sharing manners [17,32]. Due to their nucleophilic oxygen-enriched surfaces and high negative charges, POMs can serve as one type of excellent inorganic multidentate O-donor ligands for assembly of lanthanide-substituted POMs (LSPs). Hitherto, a large number of LSPs with diverse metal nuclearities, particular structural topologies and a wide range of physical and chemical properties applicable to diverse areas of research such as electronics, optics, catalysis and magnetism have been reported [33-36]. Apparently, it is comparatively difficult to explore appropriate synthetic conditions to prepare LSPs because of the two following major difficulties: (I) the disparate reaction activities of electrophilic Ln cations with nucleophilic POM precursors in a reaction system will create the unavoidable competition reaction environments; (II) Ln cations have high oxophilic reactivity towards POM fragments which usually leads to the formation of amorphous precipitates. This makes the structural determination of the products rather difficult, but we solved this problem with the hydrothermal method for the synthesis of inorganic-organic hybrids [9,13,37,38].

Thus, a new hybrid was proposed to be constructed by using a Keggin-type polyoxoanion as the inorganic building block, PDOX as the organic ligand and the Ln(III) ion as the metal linker. Unfortunately, it was found that PDOX decomposes slowly to PDA over a few days at low pH, which ruled out its use as the functional group of a solvent extractant [28,39]. Consequently, inorganic-organic hybrids constructed from the Keggin-type polyoxotungstate $[SiW_{12}O_{40}]^{4-}$ and PDA ligand linked by Ln(III) metals (Ln = Eu for 1, Er for 2) have been obtained and characterized by elemental analyses, IR spectra and single-crystal X-ray diffraction. In both compounds the lanthanoid metal center bears a high coordination number and the $[SiW_{12}O_{40}]^{4-}$ anion participates in noncovalent interactions, resulting in 3D supramolecular compounds.

EXPERIMENTAL SECTION

Materials and Instruments

All commercially available chemicals were of reagent grade and were used without further purification, except for 1,10-phenanthroline-2,9-dicarbaldehyde dioxime (H_2phendox or PDOX) which was synthesized according to a reported procedure [40,41]. All chemicals were commercially purchased and used without further purification. Elemental analyses (CHN) were performed using a Thermo Finnigan Flash-1112EA microanalyzer. The IR spectra were recorded in the range 4000-400 cm^{-1} on a Buck 500 IR spectrometer with a pressed KBr pellet. A summary of the crystallographic data and the structure refinements is provided for 1 and 2 in Table 1. Bond lengths, bond angles and other crystallographic data for these compounds are listed in Tables S1 to S14.

Synthesis and Characterization of (1)

A mixture of $H_4[SiW_{12}O_{40}]$ (144 mg, 0.05 mmol), $Eu(NO_3)_3.6H_2O$ (43.5 mg, 0.125 mmol), PDOX (33.5 mg, 0.125 mmol) and deionized water (10 ml) was stirred in air for 30 min. Then NH_4VO_3 (11 mg, 0.1 mmol) was added and the solution was stirred for an extra 30 min. Finally, the pH was adjusted to 3.5 with aqueous NaOH (1 M) solution. The mixture was then transferred into a Teflon-lined

Table 1. Crystallographic Data and Structure Refinement for 1 and 2

	1	2
Crystal data		
Chemical formula	$2(C_{56}H_{43}Eu_4N_8O_{25.50})\cdot 2(O_{40}SiW_{12})\cdot 5.5(H_2O)$	$C_{42}H_{36}Er_3N_6NaO_{61}SiW_{12}\cdot 1.5(O)\cdot 7.5(H_2O)$
M_r	9544.32	4518.94
Crystal system, space group	Monoclinic, *P*121/*c*1	Trigonal, *R*3
Temperature (K)	150	150
a, *b*, *c* (Å)	33.656 (3), 13.9520(11), 20.7047 (16)	20.288 (5), 20.288(5), 18.818 (5)
β (°)	97.6360(10)	-
V (Å^3)	9636.2 (13)	6708 (4)
Z	2	3
Radiation type	Mo $K\alpha$	Mo $K\alpha$
μ (mm^{-1})	16.94	18.28
Crystal size (mm)	0.071 × 0.204 × 0.244	0.15 × 0.08 × 0.06
Data collection		
Data with [$I > 2\sigma(I)$]	180000, 25583, 19719	44023, 8463, 7801
R_{int}	0.083	0.046
$(\sin\theta/\lambda)_{max}$ (Å^{-1})	0.689	0.709
Refinement		
$R[F^2 > 2\sigma(F^2)]$, $wR(F^2)$, S	0.079, 0.193, 1.19	0.028, 0.073, 1.02
No. of reflections	25583	8463
No. of parameters	1416	431
No. of restraints	842	259
H-atom treatment	H-atom parameters constrained	H-atom parameters constrained
$\Delta\rho_{max}$, $\Delta\rho_{min}$ (e Å^{-3})	3.33, -2.84	2.25, -1.49
Absolute structure parameter	0.015 (6)	0.015 (6)
CCDC no.	1934958	1934951

Computer programs: APEX3, SAINT, SHELXT, SHELXL-2018/1, DIAMOND [45,46].

autoclave and kept at 130 °C for 3 days. After slow cooling 2 days, the solution was filtered off and crystals could be obtained by slow evaporation of the filtrate over few weeks. Pale-yellow blade-like crystals of 1 were obtained in 58% yield (based on W). Anal. Calcd. For $C_{112}H_{98}Eu_8N_{16}O_{137}Si_2W_{24}$: C, 14.09; H, 1.03; N, 2.35%.

Found: C, 13.92; H, 1.01; N, 2.31%. IR (KBr pellet, cm^{-1}): 3423, 1613, 1568, 1468, 1388, 1307, 967, 914, 789, 712 (Fig. S4b).

Synthesis and Characterization of (2)

Compound 2 was prepared similarly to 1, except that $Er(NO_3)_3 \cdot 6H_2O$ was used in place of $Eu(NO_3)_3.6H_2O$. Yellow plate-shaped crystals were obtained in 57% yield based on $H_4SiW_{12}O_{40}$. Anal. Calcd. For $C_{42}H_{51}Er_3N_6NaO_{70}SiW_{12}$: C, 11.16; H, 1.13; N, 1.86%. Found: C, 10.92; H, 0.97; N, 1.71%. IR (KBr pellet, cm^{-1}): 3432, 1733, 1630, 1606, 1452, 1378, 1209, 916, 789, 711 (Fig. S4c).

Refinement

For 1. A specimen of $C_{112}H_{98}Eu_8N_{16}O_{137}Si_2W_{24}$, approximate dimensions 0.071 mm × 0.204 mm × 0.244 mm, was used for the X-ray crystallographic analysis. The X-ray intensity data were measured on a Bruker Smart APEX CCD system equipped with a graphite monochromator and a Mo-Kα fine-focus sealed tube (λ = 0.71073 Å). The frames were integrated with the Bruker SAINT software package using a narrow-frame algorithm. The integration of the data using a monoclinic unit cell yielded a total of 180000 reflections to a maximum θ angle of 29.32° (0.73 Å resolution), of which 25583 were independent (average redundancy 7.036, completeness = 96.9%, R_{int} = 8.27%, R_{sig} = 7.18%) and 19719 (77.08%) were greater than $2\sigma(F^2)$. The final cell constants of a = 33.656(3) Å, b = 13.9520(11) Å, c = 20.7047(16) Å, β = 97.6360(10)°, V = 9636.1(13) $Å^3$, are based upon the refinement of the XYZ-centroids of reflections above 20 σ(I). Data were corrected for absorption effects using the multi-scan method (SADABS). The calculated minimum and maximum transmission coefficients (based on crystal size) are 0.1040 and 0.3790. The structure was solved and refined using the Bruker SHELXTL Software Package, using the space group $P121/c1$, with Z = 2 for the formula unit, $C_{112}H_{98}Eu_8N_{16}O_{137}Si_2W_{24}$. The final anisotropic full-matrix least-squares refinement on F^2 with 1416 variables converged at $R1$ = 7.89%, for the observed data and $wR2$ = 19.30% for all data. The goodness-of-fit was 1.193. The largest peak in the final difference electron density synthesis was 3.331 $e^-/Å^3$ and the largest hole was -2.842 $e^-/Å^3$ with an RMS deviation of 0.403 $e^-/Å^3$. On the basis of the final model, the calculated density was 3.289 g cm^{-3} and F(000), 8572 e^-.

For 2. A specimen of $C_{42}H_{51}Er_3N_6NaO_{70}SiW_{12}$, approximate dimensions 0.063 mm × 0.082 mm × 0.153 mm, was used for the X-ray crystallographic analysis. The X-ray intensity data were measured on a Bruker Smart APEX CCD system equipped with a graphite monochromator and a Mo-Kα fine-focus sealed tube (λ = 0.71073 Å). The frames were integrated with the Bruker SAINT software package using a narrow-frame algorithm. The integration of the data using a trigonal unit cell yielded a total of 44023 reflections to a maximum θ angle of 30.24° (0.71 Å resolution), of which 8463 were independent (average redundancy 5.202, completeness = 96.8%, R_{int} = 4.57%, R_{sig} = 4.59%) and 7801 (92.18%) were greater than $2\sigma(F^2)$. The final cell constants of a = 20.288(5) Å, b = 20.288(5) Å, c = 18.818(5) Å, V = 6708.(4) $Å^3$, are based upon the refinement of the XYZ-centroids of reflections above 20 σ(I). Data were corrected for absorption effects using the multi-scan method (SADABS). The calculated minimum and maximum transmission coefficients (based on crystal size) are 0.1660 and 0.3920. The structure was solved and refined using the Bruker SHELXTL Software Package, using the space group $R3$, with Z = 3 for the formula unit, $C_{42}H_{51}Er_3N_6NaO_{70}SiW_{12}$. The final anisotropic full-matrix least-squares refinement on F^2 with 431 variables converged at $R1$ = 2.76%, for the observed data and $wR2$ = 7.27% for all data. The goodness-of-fit was 1.016. The largest peak in the final difference electron density synthesis was 2.249 $e^-/Å^3$ and the largest hole was -1.493 $e^-/Å^3$ with an RMS deviation of 0.269 $e^-/Å^3$. On the basis of the final model, the calculated density was 3.356 g cm^{-3} and F(000), 6066 e^-. The crystallographic data as well as the structure-solution and refinement details for 1 and 2 are summarized in Table 1. Detection details of the twinning and the subsequent data reduction and refinement can be found in the CIF in the supporting information.

RESULTS AND DISCUSSION

Synthesis

The successful synthesis of two compounds was accomplished by the hydrothermal reaction of lanthanoid

salts, organic ligands and $H_4SiW_{12}O_{40}.xH_2O$ as inorganic ligands. Moreover, the two main factors in synthesizing hybrid structures *i.e.* pH and temperature in this specific reaction are adjusted to about 3-3.5 and 130 °C, respectively. The mixture was stirred in air for 30 min then NH_4VO_3 was added and the solution was stirred for an extra 30 min. We think that the NH_4VO_3 is necessary for the successful isolation of crystals although it is not incorporated in the final product and its role is not clear yet. This conclusion is based on earlier reports [42-44] and initial experiments in which much amorphous precipitate and only a few poor-quality crystals were obtained by using the parent Keggin-type $H_4SiW_{12}O_{40}$ under hydrothermal conditions in the absence of NH_4VO_3. Finally, the pH was adjusted to approximately 3 with aqueous NaOH solution. The mixture was then transferred into a Teflon-lined autoclave and kept at 130 °C for 3 days. After slow cooling for about 2 days, the solution was filtered off and crystals were obtained by slow evaporation of the filtrate over few weeks. The resultant crystals are insoluble in deionized water or common organic solvents. It was found that PDOX decomposed slowly to PDA after a few days at low pH.

IR Spectroscopy

The IR spectra of compounds 1 and 2 are very similar. The presence of $[SiW_{12}O_{40}]^{4-}$ Keggin-type anions is confirmed by the characteristic vibration patterns in the region below 1000 cm^{-1}. Four bands are attributed to ῡ(Si-O_a), ῡ(W=O_t), ῡ(W-O_b), and ῡ(W-O_c) stretching vibrations which appear at averages of 922, 975, 882 and 798 cm^{-1}, respectively (where O_t = terminal oxygen, O_b = bridging oxygen, O_a = internal oxygens, and O_c = bridging oxygen atoms within the edge-sharing octahedra). Compared with the typical parent anion in $H_4[\alpha\text{-}SiW_{12}O_{40}]$, the vibrational frequencies related to the terminal oxo groups ῡ(W=O_t) are red shifted by 15 cm^{-1}. This shows that the terminal oxygen atoms (O_t) are most affected due to the coordination at the lanthanoid centers. Moreover, the vibrational band associated with ῡ(W-O_c) stretching vibration is split into two bands because of the lowered the symmetry of the Keggin anion in both compounds. The characteristic pattern in the region from 1000 to 1600 cm^{-1} is attributed to the coordinated PDA ligands. The absence of (C=O) stretching vibrations at around 1700-1720 cm^{-1} demonstrates the complete deprotonation of the carboxylic groups in the PDA ligands. Strong asymmetric and symmetric stretching frequencies for carboxylates appear at 1613 and 1388 cm^{-1}, respectively. The bands resulting from the vibrations of the aromatic skeleton also appear in the 1468 cm^{-1} region. The band centered at 3423 cm^{-1} is attributed to the ῡ(OH) vibration of the lattice and coordinated water molecules (Fig. S4).

Structure Description

X-ray structural analysis indicate that two compounds are constructed from a fundamental structural unit named $[SiW_{12}O_{40}]^{4-}$. The $[SiW_{12}O_{40}]^{4-}$ exhibits the α-Keggin structure, in which the central $\{SiO_4\}$ tetrahedron is surrounded by four vertices sharing $\{W_3O_{13}\}$ trimers. All tungsten atoms have a $\{WO_6\}$ octahedral environment and, according to the type of oxygen atom bonded to the tungsten atoms, the W-O bond lengths are divided into three groups. The W-O_c bond lengths (O_c = edge-shared oxygen atom) are the longest, the W-O_b bond lengths (O_b = corner-shared oxygen atom) are intermediate and the W-O_t bond lengths (O_t = terminal oxygen atom) are the shortest. All W(VI) centers in the compounds exhibit a $\{WO_6\}$ octahedral environment. Relevant W-O bond distances in the polyanion can be classified into three groups: W-O_c bonds, W-O_b bonds and W-O_t bonds, whose bond distances fall in the ranges 2.296 (10)-2.356 (9) Å, 1.974 (11)-1.853 (10) Å, 1.689 (11)-1.716 (10) Å for 1 and 2.27 (2)-2.401 (19) Å, 1.86 (3)-1.99 (3) Å, 1.61 (2)-1.76 (3) Å for 2, respectively. The bond angles at the W atoms vary from 72.90 (4)º to 172.0 (4)º for 1 and from 72.10 (9)º to 173.30 (10)º for 2. The central Si atom of the SiW_{12} unit is located at the inversion center and surrounded by a cube of eight oxygen atoms with each oxygen site half-occupied. The Si-O distances are in the range 1.615 (19)-1.633 (10) Å for 1 and 1.61 (2)-1.66 (2) Å for 2. The data indicate that the $\{SiO_4\}$ tetrahedra are distorted from ideal geometry. The bond lengths Ln-O (2.150 (3)-2.920 (3) Å for Eu-O in 1, 2.285 (8)-2.314 (9) Å for Er-O in 2) and Ln-N (2.460 (3)-2.582 (17) Å for Eu-N in 1, 2.446 (9)-2.449 (10) Å for Er-N in 2) around the Ln^{3+} ions are in the normal range for Ln^{3+} ions (see Tables S2, S3, S10 and S11). It is worth mentioning that variation of the Ln-O average distance along the Eu and Er series is consistent with effects of the

lanthanide contraction (ionic radius: $Eu^{3+} > Er^{3+}$). Moreover, in two compounds there exists a sequence of Ln-O distances: Ln-O (H_2O) > Ln-O_t > Ln-O (PDA), from which we can know the electron-donating ability of the oxygen atoms in three kinds of ligands that is in the order O (PDA) > O_t > O (H_2O) suggesting that the, Ln-O (PDA) bonds are more stable than the Ln-O (H_2O) and Ln-O_t bonds.

For 1. The single crystal X-ray diffraction studies revealed that hybrid 1 crystallizes in the monoclinic system in the *P*121/*c*1 space group. The asymmetric unit contains four independent Eu(III) ions, four deprotonated PDA ligands, two half Keggin-type $[SiW_{12}O_{40}]^{4-}$ (SiW_{12}) anions sitting on crystallographic centers, thirteen coordinated water molecules and five free lattice water molecules (Fig. 1). The Eu1, Eu3 and Eu4 ions are eight-coordinated with EuN_2O_6 coordination environments containing two nitrogen and three carboxyl oxygen atoms from the PDA ligands and three oxygen atoms from coordinated water molecules while Eu2 is nine-coordinated with an EuN_2O_7 coordination environment consisting of two nitrogen and three carboxyl oxygen atoms from PDA ligands and four oxygen atoms from coordinated water molecules (Fig. 1b). The overall structure is best described as composed of two different cationic layers of Eu(III) clusters with the POMs located in cavities that are created by Eu-PDA groups to finally form a 3D framework. The smallest repeating unit in layer A consist of four Eu-PDA groups which form a cyclic tetranuclear unit while in layer B, ten Eu-PDA groups generate a cyclic decanuclear unit by sharing the carboxylate oxygen atoms of their PDA ligands. Additional POMs are located in cavities in layer B. Furthermore, these positively charged 2D Eu-PDA layers are pillared by SiW_{12} anions to form a 3D microporous pillar layered framework containing guest water molecules (Fig. 2).

For 2. A view of the asymmetric unit of hybrid 2 is presented in Fig. 3. The single crystal X-ray diffraction studies reveal that hybrid 2 possesses a crystallographic C_3 axis and crystallizes in the chiral trigonal space group *R3* with a Flack parameters of 0.015 (6) (Table 1). Thus, only a third of the molecule is in the asymmetric unit. The symmetry-generated cation in 2 is composed of a cationic sodium-templated, PDA-ligated erbium(III) trimer, $\{Na[Er(PDA)(H_2O)_3]_3\}^{4+}$. This is attached to the terminal oxygen ligands of a $\{W_3O_{13}\}$ portion of the Keggin-polyanion, $[SiW_{12}O_{40}]^{4-}$ to form the basic building block of the overall structure. Each Er atom is linked by the same coordination mode that is shown in Fig. 3b. Three seven-coordinated Er(III) atoms (Er1) are coordinated by one PDA ligand through carboxyl oxygen atoms (O1) and connected by Na atom through carboxyl oxygen atoms (O2) from PDA to generate a $[Er_3(PDA)_3]$ unit. Further, Er1 is coordinated to two nitrogen (N1 and N2) and other carboxyl oxygen atom from PDA and two oxygen atoms from coordinated water molecules. The 2D metal-organic fragments and Keggin anions both are connected *via* hydrogen bonds to form interesting 3D host-guest architectures (Fig. 4).

CONCLUSIONS

Recently, studies of polyoxometalates have been improved which show that the POMs are getting increasing attention. We have successfully synthesized inorganic-organic hybrids based on the Keggin-type $[SiW_{12}O_{40}]^{4-}$ polyoxoanion building block by a rational hydrothermally synthesized approach. In this work, we have prepared and fully characterized two lanthanide-functionalized polyoxotungstates by a variety of spectroscopic techniques. These structures provide additional examples of the growing class of oxide materials designed with Keggin clusters as integral building units. The versatility of polyoxometalate clusters in general and Keggin clusters specifically in the construction of catalytic oxide materials has been amply demonstrated [4]. However, the unpredictability of the number of attachment sites on the cluster used to bridge to the secondary-metal/ligand substructure renders design principles elusive. As the data base for materials of this type expands, the structural systematics will emerge as well as a more predictable design strategy.

ACKNOWLEDGMENTS

M.M. gratefully acknowledges the financial support provided by the Ferdowsi University of Mashhad (grant No. 3/42201). We thank the Tulane Crystallography Laboratory and Universitat de les Illes Balears for collaboration.

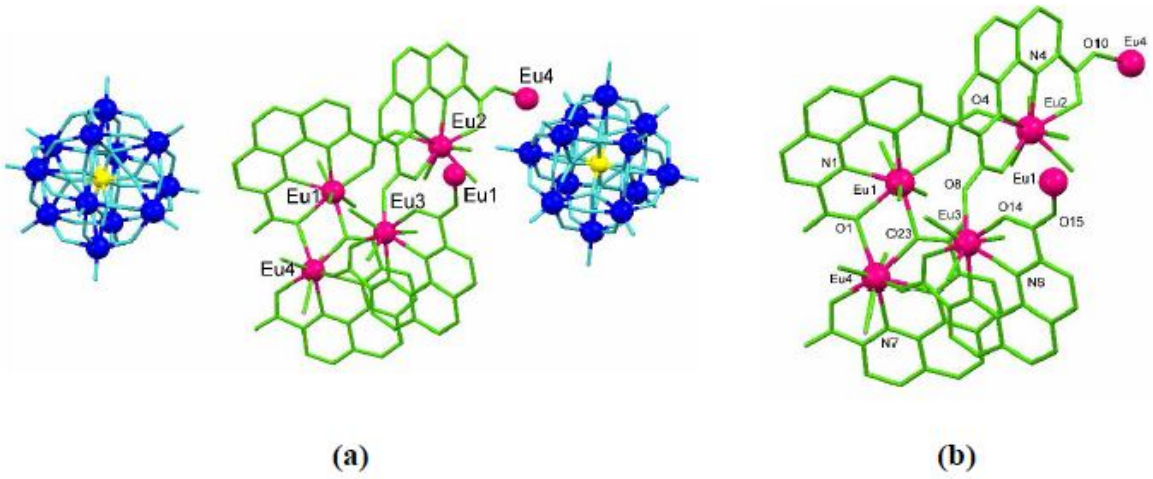

Fig. 1. (a) View of the molecular structure of 1. (b) Structure of the hexanuclear Eu(III) cluster. Crystalline water molecules and hydrogen atoms are omitted for clarity (Eu, ●; PDA, ●; POM, ●; Si, ●; O in POM, ●).

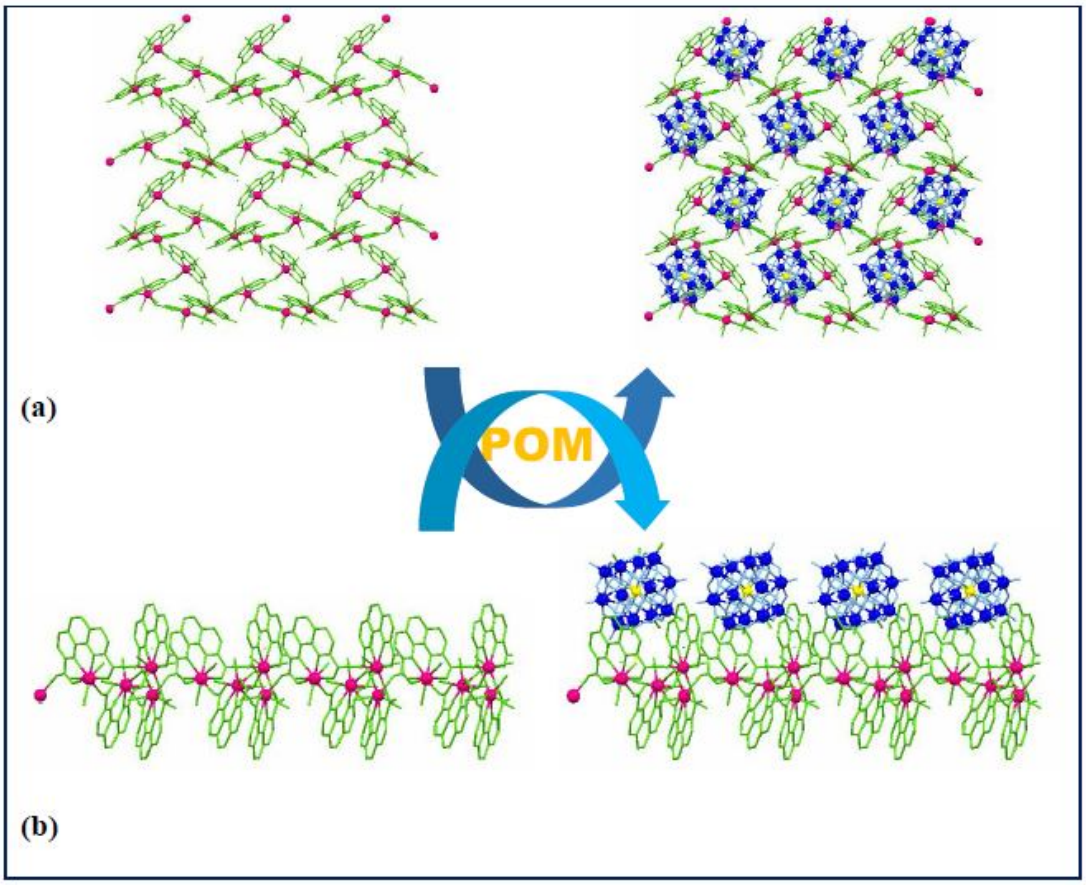

Fig. 2. Representation of the 2D Eu-PDA layer network and packing of the 3D pillar-layered framework in hybrid 1 viewed along the crystallographic a) *a* and b) *b* axis. All the water molecules trapped into the channels are omitted for clarity (Eu, ●; PDA, ●; POM, ●; Si, ●; O in POM, ●).

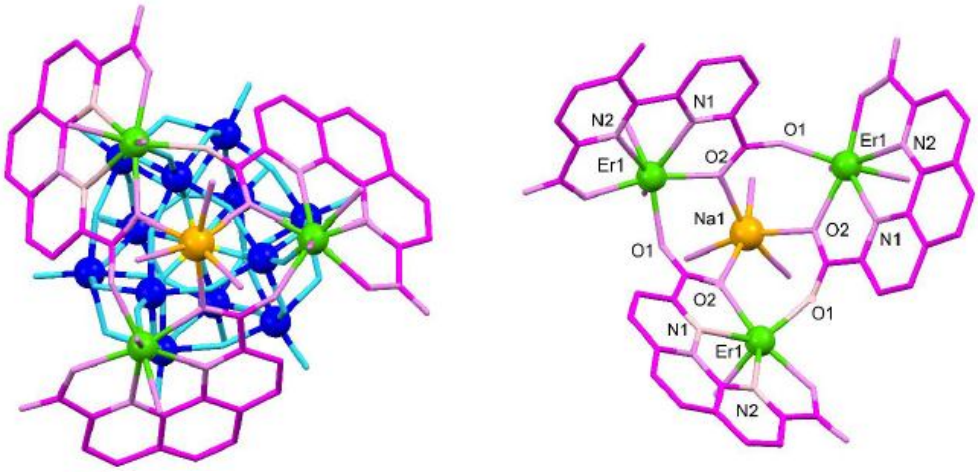

(a) **(b)**

Fig. 3. (a) View of the molecular structure of 2. (b) Structure of the trinuclear Er(III) cluster. Crystalline water molecules and hydrogen atoms are omitted for clarity (Er, ●; PDA, ●; POM, ●; Si, ●; O in POM, ●; Na, ●).

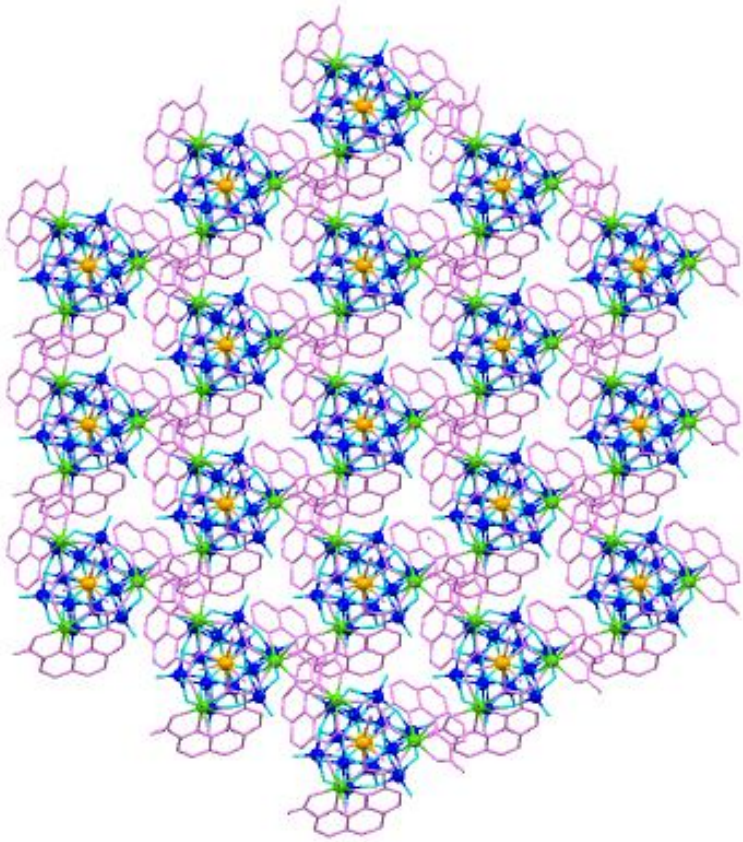

Fig. 4. View of the 3D supramolecular structure in 2 along the crystallographic *c* axis. Crystalline water molecules and hydrogen atoms are omitted for clarity (Er, ●; PDA, ●; POM, ●; Si, ●; O in POM, ●; Na, ●).

ASSOCIATED CONTENT

Supporting Information

The Supporting Information is available that including tables of selected bond lengths and bond angles for compounds, partial structural figures of compounds and IR analysis.

Accession Codes

CCDC 1934951 and 1934958 contain the supplementary crystallographic data for this paper. These data can be obtained free of charge *via* www.ccdc.cam.ac.uk/data_request/cif.

REFERENCES

[1] M.M. Heravi, M. Mirzaei, S.Y. Shirazi Beheshtiha, V. Zadsirjan, F. Mashayekh Ameli, M. Bazargan, Appl. Organometal. Chem. 32 (2018) e4479.

[2] M. Mirzaei, H. Eshtiagh-Hosseini, M. Alipour, A. Bauzá, J.T. Mague, M. Korabik, A. Frontera, Dalton Trans. 44 (2015) 8824.

[3] M. Arefian, M. Mirzaei, H. Eshtiagh-Hosseini, Inorg. Chem. Res. 1 (2016) 183.

[4] M.A. Fashapoyeh, M. Mirzaei, H. Eshtiagh-Hosseini, A. Rajagopal, M. Lechner, R. Liu, C. Streb, Chem. Commun. 54 (2018) 10427.

[5] M. Mirzaei, H. Eshtiagh-Hosseini, M. Alipour, A. Frontera, Coord. Chem. Rev. 275 (2014) 1.

[6] M. Alipour, O. Akintola, A. Buchholz, M. Mirzaei, H. Eshtiagh-Hosseini, H. Görls, W. Plass, Eur. J. Inorg. Chem. 2016 (2016) 5356.

[7] M. Arefian, M. Mirzaei, H. Eshtiagh-Hosseini, J. Mol. Struct. 1156 (2018) 550.

[8] A. Najafi, M. Mirzaei, J.T. Mague, Cryst. Eng. Comm. 18 (2016) 6724.

[9] S. Derakhshanrad, M. Mirzaei, A. Najafi, C. Ritchie, A. Bauzá, A. Frontera, J.T. Mague, Acta Cryst. C74 (2018) 1300.

[10] M. Arefian, M. Mirzaei, H. Eshtiagh-Hosseini, A. Frontera, Dalton Trans. 46 (2017) 6812.

[11] M. Mirzaei, H. Eshtiagh-Hosseini, N. Lotfian, A. Salimi, A. Bauzá, R. Van Deun, R. Decadt, M. Barceló-Oliver, A. Frontera, Dalton Trans. 43 (2014) 1906.

[12] S. Taleghani, M. Mirzaei, H. Eshtiagh-Hosseini, A. Frontera, Coord. Chem. Rev. 309 (2016) 84.

[13] N. Lotfian, M. Mirzaei, H. Eshtiagh Hosseini, M. Löffler, M. Korabik, A. Salimi, Eur. J. Inorg. Chem. 2014 (2014) 5908.

[14] M. Mirzaei, H. Eshtiagh-Hosseini, M. Arefian, F. Akbarnia, F. Miri, S. Edalatkar-Moghadam, M. Shamsipur, J. Iran. Chem. Soc. 12 (2015) 1191.

[15] N. Lotfian, M.M. Heravi, M. Mirzaei, B. Heidari, Appl. Organometal. Chem. 33 (2019) e4808.

[16] V. Goovaerts, K. Stroobants, G. Absillis, T.N. Parac-Vogt, Phys. Chem. Chem. Phys. 15 (2013) 18378.

[17] A. Proust, B. Matt, R. Villanneau, G. Guillemot, P. Gouzerh, G. Izzet, Chem. Soc. Rev. 41 (2012) 7605.

[18] J. Zhang, F. Xiao, J. Hao, Y. Wei, Dalton Trans. 41 (2012) 3599.

[19] M. Arab Fashapoyeh, M. Mirzaei, H. Eshtiagh-Hosseini, Nanochem. Res. 2 (2017) 71.

[20] W. Salomon, G. Paille, M. Gomez-Mingot, P. Mialane, J. Marrot, C. Roch-Marchal, G. Nocton, C. Mellot-Draznieks, M. Fontecave, A. Dolbecq, Cryst. Growth Des. 17 (2017) 1600.

[21] K.D. von Allmen, H. Grundmann, A. Linden, G.R. Patzke, Inorg. Chem. 56 (2016) 327.

[22] S. Herrmann, C. Ritchie, C. Streb, Dalton Trans. 44 (2015) 7092.

[23] G.A. Senchyk, A.B. Lysenko, K.V. Domasevitch, O. Erhart, S. Henfling, H. Krautscheid, E.B. Rusanov, K.W. Krämer, S. Decurtins, S.-X. Liu, Inorg. Chem. 56 (2017) 12952.

[24] G. Rousseau, L.M. Rodriguez-Albelo, W. Salomon, P. Mialane, J.r.m. Marrot, F. Doungmene, I.l.-M. Mbomekallé, P. de Oliveira, A. Dolbecq, Cryst. Growth Des. 15 (2014) 449.

[25] M. Bazargan, M. Mirzaei, M. Akbari, J. Mol. Struct. 1188 (2019) 129.

[26] M. Bazargan, M. Mirzaei, A. Franconetti, A. Frontera, Dalton Trans. 48 (2019) 5476.

[27] F. Taghipour, M. Mirzaei, Acta Cryst. C75 (2019) 231.

[28] L.L. Boone, A.E. Mroz, D.G. VanDerveer, R.D. Hancock, Eur. J. Inorg. Chem. 2011 (2011) 2706.

[29] R.D. Hancock, D.L. Melton, J.M. Harrington, F.C.

McDonald, R.T. Gephart, L.L. Boone, S.B. Jones, N.E. Dean, J.R. Whitehead, G.M. Cockrell, Coord. Chem. Rev. 251 (2007) 1678.

[30] M. Mirzaei, H. Eshtiagh-Hosseini, A. Hassanpoor, Inorg. Chim. Acta 484 (2019) 332.

[31] M. Mirzaei, A. Hassanpoor, H. Alizadeh, M. Gohari, A.J. Blake, J. Mol. Struct. 1171 (2018) 626.

[32] A. Udomvech, P. Kongrat, C. Pakawatchai, H. Phetmung, Inorg. Chem. Commun. 17 (2012) 132.

[33] L. Chen, D. Shi, Y. Wang, H. Cheng, Z. Geng, J. Zhao, P. Ma, J. Niu, J. Coord. Chem. 64 (2011) 400.

[34] D.L. Long, R. Tsunashima, L. Cronin, Angew. Chem. 49 (2010) 1736.

[35] P. Mialane, A. Dolbecq, F. Sécheresse, Chem. Commun. 33 (2006) 3477.

[36] C. Ritchie, A. Ferguson, H. Nojiri, H.N. Miras, Y.F. Song, D.L. Long, E. Burkholder, M. Murrie, P. Kögerler, E.K. Brechin, Angew. Chem. 47 (2008) 5609.

[37] W. Chen, Y. Li, Y. Wang, E. Wang, Z. Zhang, Dalton Trans. 7 (2008) 865.

[38] M. Tahmasebi, M. Mirzaei, H. Eshtiagh-Hosseini, J.T. Mague, A. Bauzá, A. Frontera, Acta Cryst. C75 (2019) 469.

[39] S. Hill, S. Datta, J. Liu, R. Inglis, C.J. Milios, P.L. Feng, J.J. Henderson, E. del Barco, E.K. Brechin, D.N. Hendrickson, Dalton Trans. 39 (2010) 4693.

[40] A. Angeloff, J.C. Daran, J. Bernadou, B. Meunier, Eur. J. Inorg. Chem. 2000 (2000) 1985.

[41] C.J. Chandler, L.W. Deady, J.A. Reiss, J. Heterocycl. Chem. 18 (1981) 599.

[42] Y. Gao, Y. Xu, Z. Han, C. Li, F. Cui, Y. Chi, C. Hu, J. Solid State Chem. 183 (2010) 1000.

[43] Z. Han, T. Chai, Y. Wang, Y. Gao, C. Hu, Polyhedron 29 (2010) 196.

[44] J. Sha, J. Peng, A. Tian, H. Liu, J. Chen, P. Zhang, Z. Su, Cryst. Growth Des. 7 (2007) 2535.

[45] O.V. Dolomanov, L.J. Bourhis, R.J. Gildea, J.A. Howard, H. Puschmann, J. Appl. Cryst. 42 (2009) 339.

[46] G.M. Sheldrick, Acta Cryst. A71 (2015) 3.